INORGANIC CHEMISTRY FRONTIERS

RESEARCH ARTICLE

View Article Online
View Journal | View Issue

Check for updates

Cite this: *Inorg. Chem. Front.*, 2023, **10**, 5303

Stapled ligand for synthesis of highly emissive and stable $CsPbBr_3$ perovskite nanocrystals in polar organic solvent†

Tianju Chen,[a] Qi Yang,[a] Peng Zhang,[a] Ruihao Chen,*[b] Yuke Lin,[a] Weifang Zhou,[a] Laizhi Sui,*[c] Xuan Zheng,*[a] Guoliang Chen[a] and Feiming Li*[a]

Colloidal cesium lead halide perovskite nanocrystals ($CsPbX_3$ PNCs) are prone to instability due to low lattice energy and dynamic ionic bonding between the PNC core and the inorganic–organic interface. To address this issue, we propose a stapled ligand, perfluoroglutaric acid (PFGA), that can effectively passivate the surface of $CsPbBr_3$ PNCs through atomic-scale double chelating coordination with Pb^{2+} between neighboring $[PbBr_6]_4^-$ unit cells. Theoretical calculations show that this precise double chelating on the surface of $CsPbBr_3$ PNCs can achieve a much stronger bonding energy (–5.19 eV) compared to single-chelated perfluoroadipic acid (–1.42 eV) or other similar ligands with trivial changes in chain length. The PFGA enables $CsPbBr_3$ PNCs to achieve a high photoluminescence quantum yield of over 85% with a single acid as a capping agent, as well as outstanding dispersion in a variety of polar solvents. Furthermore, the PFGA-capped $CsPbBr_3$ PNCs exhibit excellent purification stability after five rounds of vigorous washing and long-term stability after more than six months of storage within ethanol, which has been successfully applied for chloride sensing in different circumstances. Our findings provide insight into the design of surface engineering strategies to produce highly emissive and stable PNCs and broaden the sensing field of PNCs in polar media.

Received 10th May 2023,
Accepted 26th July 2023

DOI: 10.1039/d3qi00719g

rsc.li/frontiers-inorganic

Published on 28 July 2023. Downloaded on 2/19/2026 5:58:21 AM.

Introduction

Colloidal cesium lead halide perovskite nanocrystals ($CsPbX_3$ PNCs) are efficient semiconductors that exhibit impressive optical properties, such as near-unity photoluminescence quantum yield (PLQY), wide colour gamut, high light-absorption coefficients, and highly tunable band-edge emission.[1,2] These advantages make PNCs the system of choice for classical light emission devices, including light-emitting diodes,[3,4] lasers,[5,6] optical communication instruments,[7,8] and scintillators,[9,10] as well as promising light harvesters, such as solar cells[11,12] and photodetectors.[13,14] However, the structural instability caused by the intrinsic ionic crystal characteristics of $CsPbX_3$ PNCs has hindered their current applications. In particular, the highly dynamic interface between the PNC core and surface ligands, which typically involves proton exchange and association–dissociation processes, has been the primary challenge in obtaining sufficiently robust PNCs.[1]

On the one hand, it has been observed that protonated oleic acid (OA) and deprotonated oleyl amine (OAm) alone do not interact effectively with the surface of the PNCs. However, when the protonated N^+H group interacts with lead species (Pb-oleate, PbX_2) through hydrogen bridging bonds, it reduces their Coulomb force, ultimately resulting in the desorption of the lead oleate Z-type ligands during colloidal purification or storage.[15] These processes lead to rapid PL quenching, as well as morphological degradation and coalescence of the colloids. Therefore, various amine-free or ammonium-free methods have been developed, involving use of glycyrrhizic acid,[15] quaternary ammonium salts,[16,17] trioctylphosphine oxide,[18,19] alkylphosphonic acids,[20,21] trioctylphosphine,[22] and dodecylbenzene sulfonic acid,[23] to eliminate internal proton exchange caused by Brønsted acid–base equilibria, resulting in significant improvements in colloidal purification and stability. Additionally, use of ligands that comprise more than one functional group have been demonstrated to be an effective strategy

[a]*College of Chemistry, Chemical Engineering and Environment, Minnan Normal University, Zhangzhou, 363000, P.R. China. E-mail: lfm1914@mnnu.edu.cn, zx1974@mnnu.edu.cn*
[b]*State Key Laboratory of Solidification Processing, Center for Nano Energy Materials, School of Materials Science and Engineering, Northwestern Polytechnical University, Xi'an 710072, P. R. China. E-mail: rhchen@nwpu.edu.cn*
[c]*State Key Laboratory of Molecular Reaction Dynamics and Dalian Coherent Light Source, Dalian Institute of Chemical Physics, Chinese Academy of Sciences, Dalian, 116023 China. E-mail: lzsui@dicp.ac.cn*

†Electronic supplementary information (ESI) available: Detailed synthesis, DFT computation details and characterization of the PNCs; parameters of chloride sensing. See DOI: https://doi.org/10.1039/d3qi00719g

Published on 28 July 2023. Downloaded on 2/19/2026 5:58:21 AM.

for improving the stability of PNCs by enhancing their adsorption capacity. Bakr *et al.* utilized a bidentate ligand (2,2′-iminodibenzoic acid (IDA)) to simultaneously passivate two surface-exposed Pb atoms, resulting in a larger binding energy of 1.4 eV compared to that of the single carboxylic OA ligand with 1.14 eV. This allowed the IDA-treated $CsPbI_3$ PNCs to exhibit a high PLQY of 95% and improved stability.[24] Kovalenko *et al.* used a zwitterionic soy lecithin as capping ligands to maintain the structural integrity of $CsPbBr_3$ PNCs over a wide range of concentrations.[25] More recently, Snaith *et al.* employed multidentate ligands, namely ethylenediaminetetraacetic acid (EDTA) and reduced L-glutathione, to "clean" the lead atoms of mixed-halide PNC surfaces, which suppressed the formation of iodine Frenkel defects and inhibited halide segregation.[26] These results demonstrate the excellent potential of polydentate ligands for improving the stability and optical properties of PNCs. Interestingly, multidentate ligands with functional groups spaced more than eight atoms apart have seldom been reported for passivation of PNCs due to incomplete passivation resulting from inappropriate bonding sites. Spatial matching between the ligand functional group sites and PNC surfaces is also a key parameter for the design of ligands, although it has not been taken seriously so far, as more desirable binding energy can be achieved by eliminating unnecessary energy loss from molecular geometrical distortion.

In this study, we propose a novel approach to passivate the surface of $CsPbBr_3$ PNCs using a stapled ligand, perfluoroglutaric acid (PFGA). The bidentate positions of PFGA are highly matched to the cubic $CsPbBr_3$ lattice parameter at an atomic level, where Pb^{2+}–Pb^{2+} interaction between neighboring $[PbBr_6]_4^-$ unit cells is stapled *via* a bidentate coordination approach (see Scheme 1), allowing for precise passivation of the PNC surface. Our first-principles density functional theory (DFT) calculations confirm that the surface of $CsPbBr_3$ PNCs precisely double-chelated with PFGA possesses much stronger bonding than that with single-chelated ligands or similar double-chelated ligands, even with a difference of only one atom. Moreover, $CsPbBr_3$ PNCs passivated with PFGA using only a single ligand display a high PLQY of over 85% with outstanding dispersion and stability in a variety of polar organic solvents. The strong bonding energy and exposed hydrophilic carboxyl interface of PFGA effectively passivate the $CsPbBr_3$ PNC surface, making this an effective and promising approach for improving the stability and optical properties of PNCs. Our results suggest that the spatial matching between ligand functional group sites and PNC surface is a critical parameter for designing ligand molecules and should be taken into account to achieve desirable binding energy while minimizing unnecessary energy loss from molecular geometrical distortion.

Results and discussion

In this study, we investigated the effectiveness of a proposed stapled ligand for the synthesis of highly emissive $CsPbBr_3$ PNCs. We synthesized $CsPbBr_3$ PNCs using a series of ligands as capping agents, namely perfluoroglutaric acid (PFGA), perfluorovaleric acid (PFVA), perfluorosuccinic acid (PFSA), and perfluoroadipic acid (PFAA), as shown in Fig. 1a. We found that only PFGA was an appropriate ligand for the synthesis of $CsPbBr_3$ PNCs, despite the similarity in molecular structures of these ligands. We ruled out the possibility of partial PFGA binding on the $CsPbBr_3$ surface through single chelating coordination by comparing the PFGA and PFVA cases. To gain further insights into the underlying mechanism, we calculated

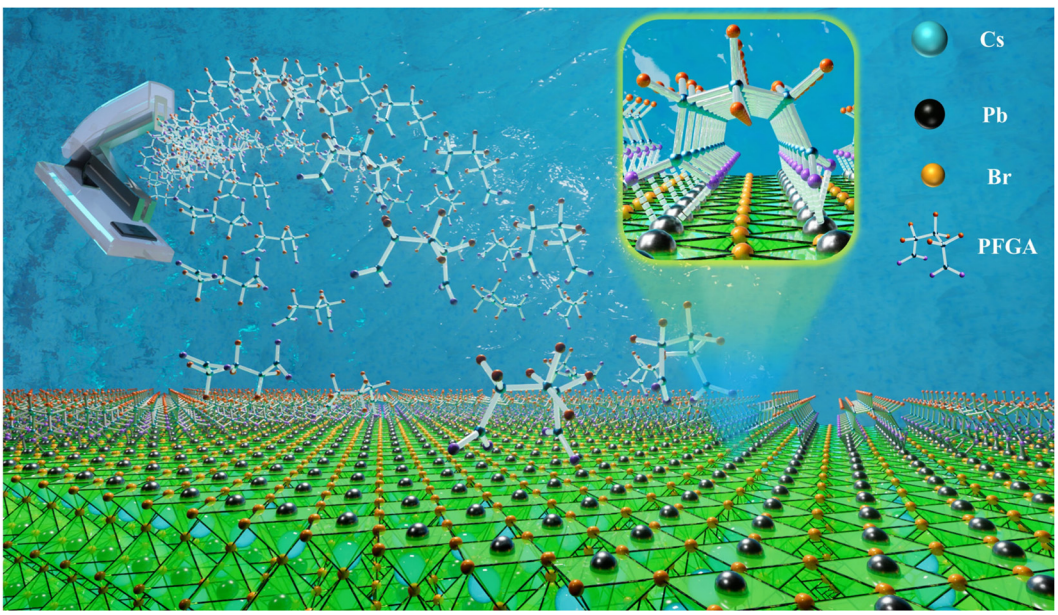

Scheme 1 Schematic depiction of the PFGA stapled ligand on $CsPbBr_3$ PNCs in polar organic solvent.

 This journal is © the Partner Organisations 2023

Published on 28 July 2023. Downloaded on 2/19/2026 5:58:21 AM.

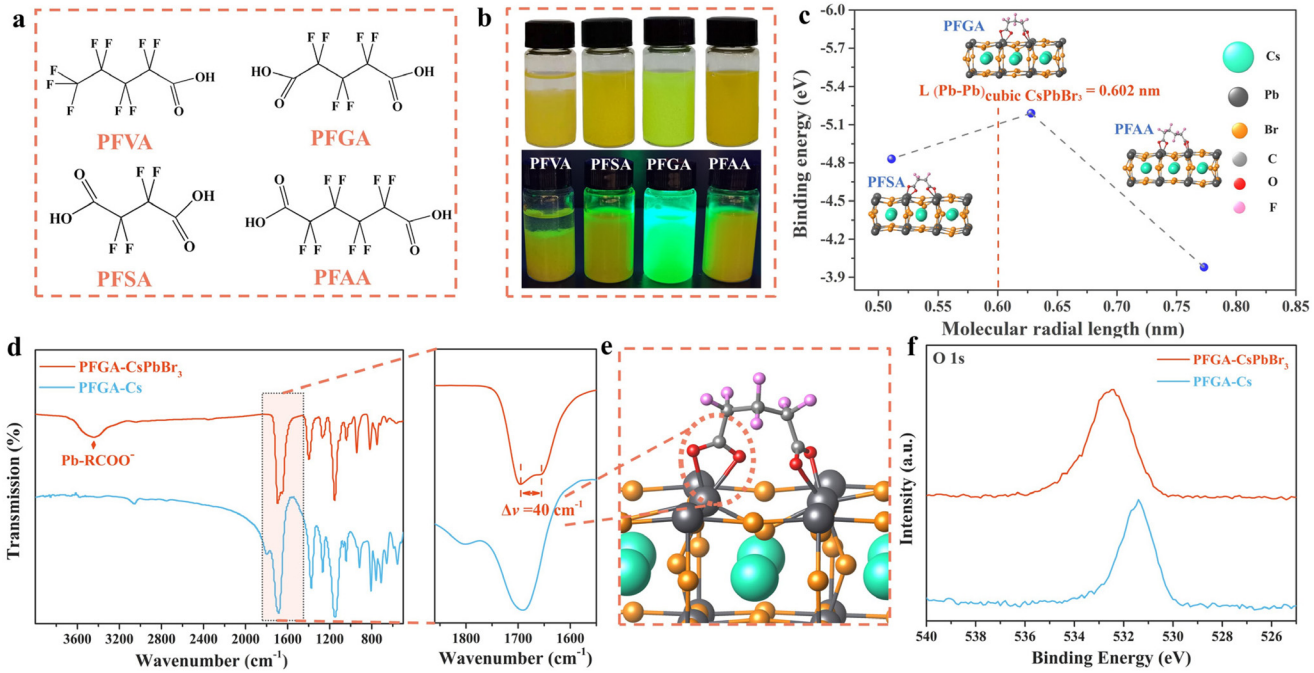

Fig. 1 (a) Structural formulas of PFVA, PFGA, PFSA, and PFAA. (b) Photograph of $CsPbBr_3$ PNCs using PFVA, PFGA, PFSA, and PFAA as ligands under normal white light (above) and a 365 nm UV (below). (c) Size effects of $CsPbBr_3$ PNCs on the binding energy and space matching. (d) FTIR spectra and their partial magnification in the COO^- region of Cs_2PFGA and PFGA-$CsPbBr_3$ PNCs. (e) Atomic structure of an optimized $CsPbBr_3$ (001) surface with the PFGA molecule. (f) The high-resolution O 1s spectra of Cs_2PFGA and PFGA-$CsPbBr_3$ PNCs.

the binding energy of each adsorbate by DFT methods (see ESI† for computational details). During the calculation process, we also considered PFSA and PFAA as having double chelating coordination since their single chelating coordination is similar to that of PFVA. We found that PFGA was anchored at two surface-adjacent Pb atoms on the optimized $CsPbBr_3$ (001) surface with a larger binding energy (−5.19 eV) than those of the PFSA/PFAA/PFVA cases (−4.83 eV/−3.98 eV/−1.42 eV, respectively), indicating that the strongest stability of the chelate bonds was that between Pb^{2+} and carboxyl (COO^-) of PFGA. This strong stability may be due to the molecular size of PFGA being the most suitable, where the optimized molecular radial length of PFGA (6.33 Å) is well matched with the edge length of the $CsPbBr_3$ cell (*i.e.*, Pb–Br–Pb, 6.02 Å). In contrast, the radial length of PFSA or PFAA (5.17 Å or 7.75 Å) appears to be too short or too long, respectively (see Fig. 1c).

To gain a deeper understanding of how PFGA affects the NC surface, Fourier-transform infrared (FTIR) spectra and X-ray photoelectron spectroscopy (XPS) spectra were acquired for Cs_2PFGA and PFGA-$CsPbBr_3$ PNCs. As shown in Fig. 1d, the absorption peaks of PFGA-$CsPbBr_3$ PNCs were similar to those of Cs_2PFGA, except for a strong band at the 3200–3600 cm^{-1} region corresponding to the coordinate bond of COO^- and Pb^{2+}. This confirms the existence of chelating agents on the PNC surface. These results were consistent with those of the full-scan XPS spectrum, in which all the related ligand elements can be observed above the detection limits (Fig. S1†). Compared to Cs_2PFGA, the antisymmetric stretching vibrations $\nu_{as}(COO^-)$ and symmetric stretching vibrations $\nu_s(COO^-)$ of the PFGA-$CsPbBr_3$ PNCs were shifted from 1803 and 1691 cm^{-1} to 1696 and 1656 cm^{-1}, respectively (Fig. 1d). The frequency difference ($\Delta\nu = \nu_{as} - \nu_s$) of PNCs reducing by 40 cm^{-1} revealed the chelating geometry of the dicarboxylic acid moiety under their variation of bond order (Fig. 1e).[27] Furthermore, the high-resolution XPS spectrum showed that the O 1s signal of PFGA-$CsPbBr_3$ PNCs shifted from 532.5 eV to 531.4 eV (Fig. 1f). The large low-field offset indicates the stronger interaction between PFGA and $CsPbBr_3$ surface, as well as the electron-donating coordination from carboxyl.

The PFGA-$CsPbBr_3$ PNCs were synthesized using a modified ligand-assisted precipitation method (see detailed methods in the ESI† and related Fig. 2a).[28] In this method, equimolar amounts of cesium perfluoroglutarate (Cs_2PFGA) and $PbBr_2$ were dissolved in DMSO to prepare the precursor, which was then injected into ethanol under magnetic stirring using a water bath at 25 °C. Despite the shortage of bromine ions and the use of a single acid as ligand, the PFGA-$CsPbBr_3$ PNCs exhibited a relatively high QY of 86% (Fig. 2d). Previous approaches that used only acid molecules as additives for surface ligands resulted in enormous negatively charged defects due to charge competition,[16] leading to a low QY generated from the negative exciton trapping effect of the halogen vacancy.[29]

We believe that the relatively high QY of the resulting PNCs can be attributed mainly to the precise passivation and little

Published on 28 July 2023. Downloaded on 2/19/2026 5:58:21 AM.

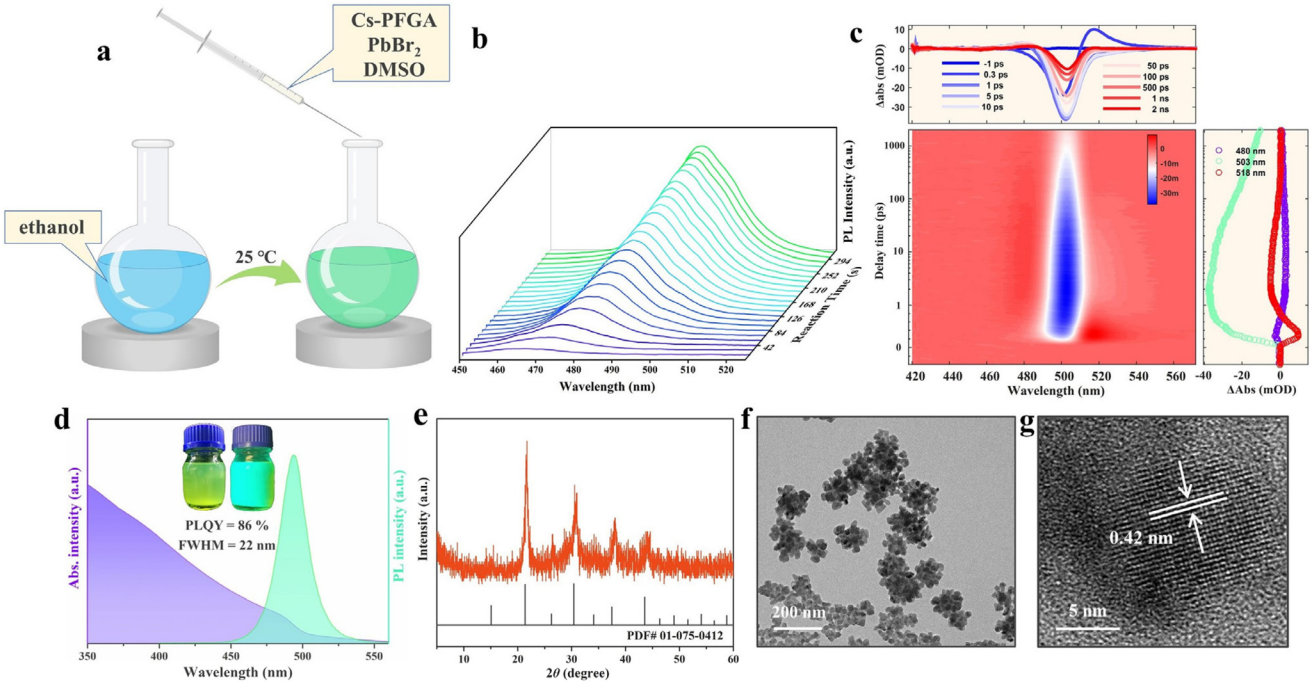

Fig. 2 (a) Schematic depiction of the ligand-assisted precipitation method of PFGA-$CsPbBr_3$ PNCs. (b) *In situ* PL spectra during the precipitation process. (c) TA spectra taken at several representative probe delays. (d) Absorption (purple area) and PL (green area) spectra of PFGA-$CsPbBr_3$ PNCs. Inset: photograph showing the PFGA-$CsPbBr_3$ PNCs in ethanol solution under (left) normal white light and (right) 365 nm UV light. (e) XRD pattern; (f) TEM image and (g) HR-TEM image of the PFGA-$CsPbBr_3$ PNCs.

steric repulsion in stapled PFGA, which can effectively remove most of the lead atoms on the PNC surface. Furthermore, the *in situ* PL spectrum shown in Fig. 2b demonstrates that the PFGA-assisted precipitation process involves a rapid nucleation and several minutes of slow growth due to the weak interfacial tension between polar anti-solvent and ionic crystals, which reduces the reactivity of crystal growth. In contrast, classic precipitation typically completes nucleation and growth within several seconds.[28] It is worth noting that the slow growth process seems to promote the crystalline structural integrity and optical performance of the PNCs, as a growth rate that is too fast may not be able to compensate for all the missing bromide ions in the $[PbBr_6]^{4-}$ octahedra.[29] Therefore, the different precipitation process may also be an important factor influencing the optical performance of the PFGA-$CsPbBr_3$ PNCs. We measured the ultrafast dynamics of PFGA-$CsPbBr_3$ PNCs dispersed in ethanol using femtosecond transient absorption (TA). Within the first 1 ps, the photon-induced absorption (PIA) at 518 nm decayed immediately, and the ground state bleaching (GSB) at 505 nm began to increase, which was caused by the relaxation of hot carriers. The absence of an obvious GSB signal in the low-energy region indicates that the trap states are effectively passivated.[30]

Transmission electron microscopy (TEM) images revealed that PFGA-$CsPbBr_3$ PNCs tend to form loose and irregular clusters (Fig. 2f) due to the lack of stereoscopic barrier on PFGA ligands and the low surface energy of $-CF_3$ and $-CF_2-$ groups (16 and 18 mN M^{-1}, respectively).[31] The practical particle size distribution of the PNCs was around 120 nm, as measured by dynamic light scattering (DLS) (Fig. S2†), which is consistent with the TEM image. The PFGA-$CsPbBr_3$ PNCs exhibited a green PL peak at 500 nm with a full width at half-maximum of 22 nm (Fig. 2d). The obvious quantum confinement effect in the PL peak suggests that the PNCs are individual aggregates rather than being fused together. X-ray diffraction (XRD) patterns of PFGA-$CsPbBr_3$ PNCs showed that their diffraction peaks match well with the cubic phase of $CsPbBr_3$ (standard card, ICSD#01-075-0412) (Fig. 2e). Moreover, the lattice spacing of 4.2 Å observed in the high-resolution TEM (HR-TEM) image, corresponding to the (110) crystal plane of the cubic $CsPbBr_3$, further confirms the crystalline phase of the $CsPbBr_3$ PNCs (Fig. 2g).

Theoretical calculations suggest that the ligands bind tightly to the $CsPbBr_3$ PNCs, resulting in excellent stability and dispersion in various polar solvents. The orientation forces between the exposed hydrophilic carboxyl group and solvent molecules contribute to the dispersity in polar solvents. However, this dispersity comes at the cost of poor deposition in non-polar solvents, as illustrated in Fig. S3.† To demonstrate the stability of PFGA-$CsPbBr_3$ PNCs, we compared their photoluminescence (PL) emission with that of OA/OAm-capped $CsPbBr_3$ PNCs in ethanol over a period of two months. While the PL intensity of OA/OAm-$CsPbBr_3$ PNCs rapidly quenched within 5 min, PFGA-$CsPbBr_3$ PNCs showed no significant difference in PL intensity even after 60 days (Fig. 3a). This indicates a strong interaction between PFGA and the PNC

 This journal is © the Partner Organisations 2023

Published on 28 July 2023. Downloaded on 2/19/2026 5:58:21 AM.

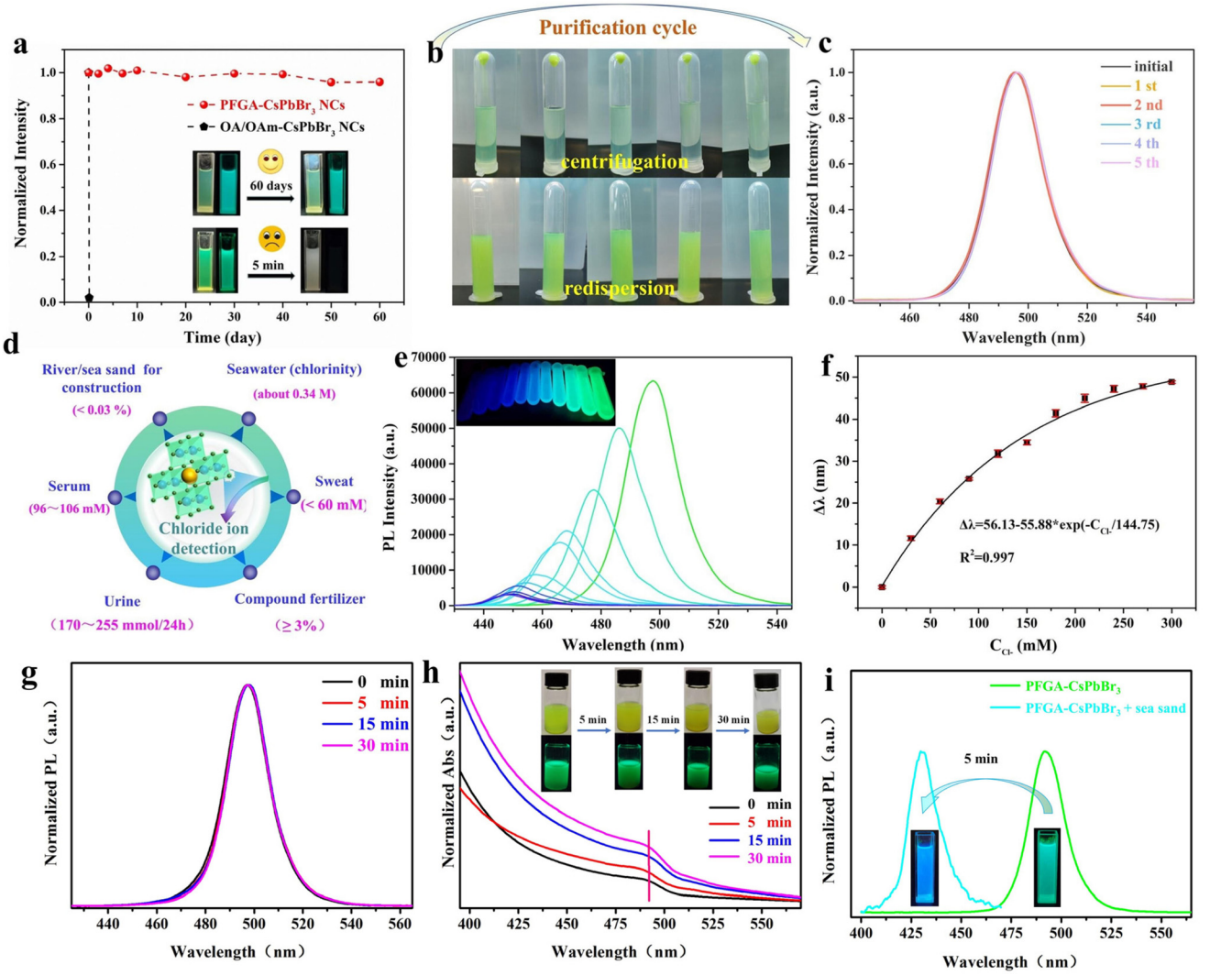

Fig. 3 (a) Long-term stability of PFGA-$CsPbBr_3$ PNCs. (b) Photograph under daylight and (c) corresponding normalized PL spectra of PFGA-$CsPbBr_3$ PNCs after 1–5 washing cycles with ethanol. (d) Common application in chlorine ion detection. (e) Fluorescence spectra of PFGA-$CsPbBr_3$ PNC solutions with the addition of different concentrations of Cl^- from 0 to 330 mM. Inset in (e) shows corresponding fluorescence photographs under 365 nm UV excitation. (f) The working curve of the established sensing system. (g, h) The normalized PL; and UV absorption spectra of PFGA-$CsPbBr_3$ PNCs reacting with river sand. (i) The normalized PL spectra of PFGA-$CsPbBr_3$ PNCs reacting with sea sand.

surface. Another important issue for practical applications is the purification problem caused by the highly dynamic OA and OAm, which easily escape from the surface of NCs. During purification of OA/OAm-$CsPbBr_3$ PNCs in toluene, imperfect passivation and particle aggregation caused the PL spectra to gradually redshift and impure peaks to appear (Fig. S4†). In contrast, after violent washing of PFGA-$CsPbBr_3$ PNCs with ethanol five times, there was no significant difference in product color, colloidal dispersibility, or fluorescence emission (Fig. 3b and c), which further demonstrates the strong adsorption capacity of PFGA and its outstanding stability, and the fact that PFGA-$CsPbBr_3$ PNCs retain their excellent optical properties even after long-term storage and multiple washing. Compared with the other ligands for the synthesis of $CsPbX_3$ PNCs (especially for $CsPbBr_3$ PNCs) summarized in Table S2,† PFGA served as a powerful ligand for the synthesis of $CsPbBr_3$ PNCs in polar solvents with high stability and PLQY, compared with the other ligands.

The susceptibility of the intrinsic ionic structure of PNCs to ionic attack and the tendency of ion migration to occur in a polar environment make the polar stability and dispersion of PFGA-$CsPbBr_3$ PNCs ideal for use as a fluorescent probe for ion detection, especially for the chloride ion (Cl^-). Cl^- can rapidly and selectively react with the $CsPbBr_3$ PNCs by halogen exchange due to the low vacancy diffusion activation energy of halides ($CsPbBr_3$ and $CsPbCl_3$ have activation energies of 0.25 eV and 0.29 eV, respectively).[32] The detection of Cl^- is of great significance in practical applications due to its important industrial uses and physiological functions, as highlighted in previous studies (Fig. 3d).[33–35] Here, we showcase two

Published on 28 July 2023. Downloaded on 2/19/2026 5:58:21 AM.

common instances of homogeneous and heterogeneous Cl^- detection using a PFGA-$CsPbBr_3$ PNC ethanol solution.

To detect Cl^- in aqueous solutions, such as urine samples, homogeneous detection can be used. To optimize the system stability and reaction time, several key parameters were adjusted, as shown in Fig. S5 and S6.† The relationship between the PL wavelength and the concentration of Cl^- was then examined, as shown in Fig. 3e. The wavelength shift $\Delta\lambda$ (where $\Delta\lambda = \lambda_0 - \lambda$, and λ_0 and λ represent the PL wavelength of PNCs before and after the addition of Cl^-) displayed a good linear relationship with Cl^- concentration ranging from 0–300 mM (Fig. 3f). The XRD pattern in Fig. S7† shows the structure of PFGA-$CsPbBr_3$ PNCs after addition of Cl^- and has been investigated, and the relative XRD pattern is shown subsequently. We could find that as Cl^- increased, the characteristic peaks of the products still retain the cubic $CsPbBr_3$ phase with a small amount of $CsPb_2Br_5$ phase, and all the peaks shifted to higher angles, which might be ascribed to the cell being shrunk upon incorporation of Cl^-, which is consistent with the results reported in previous work.[2] Besides, the PL lifetime changes of $CsPbBr_3$ PNCs after halide exchange have been investigated (Fig. S8†). Results showed that contrary to previously reported results, the fluorescence lifetime increased with increasing chloride ion concentration, since the proportion of $\tau 3$ increased with increasing Cl^- concentration, indicating a nonradiative recombination process (such as surface traps or/and bulk defect-related traps).[1,2] The prepared system demonstrated good selectivity and anti-interference ability, as shown in Fig. S9.† Direct detection was carried out on urine samples obtained from three healthy volunteers without any pretreatment. The results showed relative standard deviations (RSD) ranging from 1.8% to 2.3% and recovery rates in the range of 94%–106% (Table S3†), indicating the reliability and reproducibility of the detection results. The comparison of chloride sensing in different solvents has been summarized in Table S4.† The results show that the ligand in $CsPbBr_3$ PNCs plays a decisive role in the detection of chloride ions, and when polar-stabilized $CsPbBr_3$ PNCs are used, chloride ions can be detected by homogeneous determination, and in contrast, when non-polar-stabilized $CsPbBr_3$ PNCs are used, chloride ions can only be detected by non-homogeneous determination, and the diffusion of chloride ions needs to be accelerated through magnetic stirring,[36] which makes the steps relatively cumbersome.

The ability of PFGA-$CsPbBr_3$ PNCs to qualitatively detect Cl^- in solids, such as in river/sea sand, is of great importance in the construction industry. This is because the use of sea sand in construction can lead to the formation of soluble metal ions due to the enrichment of Cl^-, which can cause corrosion of stainless steel and ultimately affect the lifespan of the building. The traditional method for detecting Cl^- in solids using silver ions is expensive and time-consuming, but PFGA-$CsPbBr_3$ PNCs provide a simple, efficient, and visualized identification platform. When river/sea sand is introduced into an ethanol solution of PFGA-$CsPbBr_3$ PNCs, the system shows no response to river sand (Fig. 3g and h), but sea sand causes a pronounced color change and a wide wavelength blue-shift within minutes (Fig. 3i and Fig. S6†), demonstrating the potential of this system for practical applications.

Conclusions

In summary, we have successfully passivated the surface of $CsPbBr_3$ PNCs through atomic-scale double chelating coordination with Pb^{2+} between neighbouring $[PbBr_6]_4^-$ unit cells using the stapled ligand PFGA. This has resulted in precise passivation of the $CsPbBr_3$ PNC surface and strong bonding energy. Both theoretical and experimental results have confirmed the size matching and double-chelated mechanism of PFGA, which has enabled excellent optical performance of the PFGA-$CsPbBr_3$ PNCs under a single acid as ligand. Specifically, we have demonstrated the ability of PFGA-$CsPbBr_3$ PNCs to serve as robust fluorescent probes for real-time and on-site detection of Cl^-. In addition, we have shown that homogeneous detection of chlorine in urine can be achieved using an ethanol solution of PFGA-$CsPbBr_3$ PNCs, with reliable and reproducible results. Furthermore, we have demonstrated that this solution can also rapidly identify river/sea sand heterogeneously within several minutes. Our work sheds light on the spatial correlation between the crystal plane of PNCs and the binding site of a polydentate ligand, and has broadened the sensing field of PNCs in polar media.

Author contributions

Tianju Chen: Methodology, investigation, writing – original draft. Qi Yang: Data curation. Peng Zhang: Validation. Ruihao Chen: Supervision, investigation. Yuke Lin: Resources, supervision. Weifang Zhou: Supervision, investigation. Laizhi Sui: Theoretical calculations. Xuan Zhen: Theoretical calculations. Guoliang Chen: Resources, project administration. Feiming Li: Supervision, project administration, funding acquisition.

Conflicts of interest

There are no conflicts to declare.

Acknowledgements

We gratefully acknowledge the financial support of the National Natural Science Foundation of China (No. 22004055) and Natural Science Foundation of Fujian Province of China (2020J05165).

References

1 N. F. Maneiro, K. Sun, L. L. Fernández, S. G. Graña, P. M. Buschbaum and L. Polavarapu, Ligand chemistry of

 This journal is © the Partner Organisations 2023

Published on 28 July 2023. Downloaded on 2/19/2026 5:58:21 AM.

inorganic lead halide perovskite nanocrystals, *ACS Energy Lett.*, 2023, **8**, 1152–1191.

2 Q. A. Akkerman, G. Rainò, M. V. Kovalenko and L. Manna, Genesis, Genesis, challenges and opportunities for colloidal lead halide perovskite nanocrystals, *Nat. Mater.*, 2018, **17**, 394–405.

3 M. Liu, Q. Wan, H. Wang, F. Carulli, X. Sun, W. Zheng, L. Kong, Q. Zhang, C. Zhang, Q. Zhang, S. Brovelli and L. Li, Suppression of temperature quenching in perovskite nanocrystals for efficient and thermally stable light-emitting diodes, *Nat. Photonics*, 2021, **15**, 379–385.

4 L. Jing, Q. Xie, H. Li, K. Li, H. Yang, P. L. P. Ng, S. Li, Y. Li, E. H. T. Teo, X. Wang and P.-Y. Chen, Multigenerational crumpling of 2D materials for anticounterfeiting patterns with deep learning authentication, *Matter*, 2020, **3**, 2160–2180.

5 Y. H. Hsieh, B.-W. Hsu, K.-N. Peng, K.-W. Lee, C. W. Chu, S.-W. Chang, H.-W. Lin, T.-J. Yen and Y.-J. Lu, Perovskite quantum dot lasing in a gap-plasmon nanocavity with ultralow threshold, *ACS Nano*, 2020, **14**, 11670–11676.

6 S. Li, D. Lei, W. Ren, X. Guo, S. Wu, Y. Zhu, A. L. Rogach, M. Chhowalla and A. K. Y. Jen, Water-resistant perovskite nanodots enable robust two-photon lasing in aqueous environment, *Nat. Commun.*, 2020, **11**, 1192.

7 M. Xia, S. Zhu, J. Luo, Y. Xu, P. Tian, G. Niu and J. Tang, Ultrastable perovskite nanocrystals in all-Inorganic transparent Matrix for high-Speed underwater wireless optical communication, *Adv. Opt. Mater.*, 2021, **9**, 2002239.

8 X. Pan, J. Zhang, H. Zhou, R. Liu, D. Wu, R. Wang, L. Shen, L. Tao, J. Zhang and H. Wang, A nano-micro engineering nanofiber for electromagnetic absorber, green shielding and sensor, *Nano-Micro Lett.*, 2021, **13**, 70.

9 H. Zhang, Z. Yang, M. Zhou, L. Zhao, T. Jiang, H. Yang, X. Yu, J. Qiu, Y. Yang and X. Xu, Reproducible X-ray imaging with a perovskite nanocrystal scintillator embedded in a transparent amorphous network structure, *Adv. Mater.*, 2021, **33**, 2102529.

10 Q. Chen, J. Wu, X. Ou, B. Huang, J. Almutlaq, A. A. Zhumekenov, X. Guan, S. Han, L. Liang, Z. Yi, J. Li, X. Xie, Y. Wang, Y. Li, D. Fan, D. B. L. Teh, A. H. All, O. F. Mohammed, O. M. Bakr, T. Wu, M. Bettinelli, H. Yang, W. Huang and X. Liu, All-inorganic perovskite nanocrystal scintillators, *Nature*, 2018, **561**, 88–93.

11 W. Sun, R. Yun, Y. Liu, X. Zhang, M. Yuan, L. Zhang and X. Li, Ligands in Lead Halide perovskite nanocrystals: from synthesis to optoelectronic applications, *Small*, 2023, **19**, 2205950.

12 Y. Chen, N. Wei, Y. Miao, H. Chen, M. Ren, X. Liu and Y. Zhao, Inorganic $CsPbBr_3$ perovskite nanocrystals as interfacial ion reservoirs to stabilize $FAPbI_3$ perovskite for efficient photovoltaics, *Adv. Energy Mater.*, 2022, **12**, 2200203.

13 D. Liu, Y. Guo, M. Que, X. Yin, J. Liu, H. C. Zhang and W. Que, Metal halide perovskite nanocrystals: application in high-performance photodetectors, *Mater. Adv.*, 2021, **2**, 856–879.

14 C. Kang, I. Dursun, G. Liu, L. Sinatra, X. Sun, M. Kong, J. Pan, P. Maity, E. Ooi, T. Ng, O. Mohammed, O. Bakr and B. Ooi, High-speed colour-converting photodetector with all-inorganic $CsPbBr_3$ perovskite nanocrystals for ultraviolet light communication, *Light: Sci. Appl.*, 2019, **8**, 94.

15 L. L. Zheng, K. Y. Jiang, X. L. Li, P. B. Hong, K. Chen, H. Zhang, Y. B. Song and B. B. Luo, Water-assisted preparation of ethanol-dispersed $CsPbBr_3$ perovskite nanocrystals and emissive gel, *J. Colloid Interface Sci.*, 2021, **598**, 166–171.

16 E. Yassitepe, Z. Yang, O. Voznyy, Y. Kim, G. Walters, J. A. Castañeda, P. Kanjanaboos, M. Yuan, X. Gong, F. Fan, J. Pan, S. Hoogland, R. Comin, O. M. Bakr, L. A. Padilha, A. F. Nogueira and E. H. Sargent, Amine-free synthesis of cesium lead halide perovskite quantum dots for efficient light-emitting diodes, *Adv. Funct. Mater.*, 2016, **26**(47), 8757–8763.

17 Y. Tan, Y. Zou, L. Wu, Q. Huang, D. Yang, M. Chen, M. Ban, C. Wu, T. Wu, S. Bai, T. Song, Q. Zhang and B. Sun, Highly luminescent and stable perovskite nanocrystals with octylphosphonic acid as a ligand for efficient light-emitting diodes, *ACS Appl. Mater. Interfaces*, 2018, **10**(4), 3784–3792.

18 B. Zhang, L. Goldoni, J. Zito, Z. Dang, G. Almeida, F. Zaccaria, J. de Wit, I. Infante, L. De Trizio and L. Manna, Alkyl phosphonic acids deliver $CsPbBr_3$ nanocrystals with high photoluminescence quantum yield and truncated octahedron shape, *Chem. Mater.*, 2019, **31**(21), 9140–9147.

19 H. Wang, N. Sui, X. Bai, Y. Zhang, Q. Rice, F. J. Seo, Q. Zhang, V. L. Colvin and W. W. Yu, Emission recovery and stability enhancement of inorganic perovskite quantum dots, *J. Phys. Chem. Lett.*, 2018, **9**(15), 4166–4173.

20 C. Lu, H. Li, K. Kolodziejski, C. Dun, W. Huang, D. Carroll and S. M. Geyer, Enhanced stabilization of inorganic cesium lead triiodide ($CsPbI_3$) perovskite quantum dots with tri-octylphosphine, *Nano Res.*, 2018, **11**(2), 762–768.

21 F. Liu, Y. Zhang, C. Ding, K. Kawabata, Y. Yoshihara, T. Toyoda, S. Hayase, T. Minemoto, R. Wang and Q. Shen, Trioctylphosphine oxide acts as alkahest for SnX_2/PbX_2: A general synthetic route to perovskite $ASn_xPb_{1-x}X_3$ (A=Cs, FA, MA; X=Cl, Br, I) quantum dots, *Chem. Mater.*, 2020, **32**(3), 1089–1100.

22 G. Almeida, O. J. Ashton, L. Goldoni, D. Maggioni, U. Petralanda, N. Mishra, Q. A. Akkerman, I. Infante, H. J. Snaith and L. Manna, The phosphine oxide route toward lead halide perovskite nanocrystals, *J. Am. Chem. Soc.*, 2018, **140**(44), 14878–14886.

23 D. Yang, X. Li, W. Zhou, S. Zhang, C. Meng, Y. Wu, Y. Wang and H. Zeng, $CsPbBr_3$ quantum dots 2.0: benzenesulfonic acid equivalent ligand awakens complete purification, *Adv. Mater.*, 2019, **31**(30), e1900767.

24 J. Pan, Y. Shang, J. Yin, M. De Bastiani, W. Peng, I. Dursun, L. Sinatra, A. M. El-Zohry, M. N. Hedhili, A.-H. Emwas, O. F. Mohammed, Z. Ning and O. M. Bakr, Bidentate ligand-passivated $CsPbI_3$ perovskite nanocrystals for stable near-unity photoluminescence quantum yield and efficient red light-emitting diodes, *J. Am. Chem. Soc.*, 2018, **140**(2), 562–565.

Published on 28 July 2023. Downloaded on 2/19/2026 5:58:21 AM.

25 F. Krieg, Q. K. Ong, M. Burian, G. Rainò, D. Naumenko, H. Amenitsch, A. Süess, M. J. Grotevent, F. Krumeich, M. I. Bodnarchuk, I. Shorubalko, F. Stellacci and M. V. Kovalenko, Stable ultraconcentrated and ultradilute colloids of $CsPbX_3$ (X=Cl, Br) nanocrystals using natural lecithin as a capping ligand, *J. Am. Chem. Soc.*, 2019, **141**(50), 19839–19849.

26 Y. Hassan, J. H. Park, M. L. Crawford, A. Sadhanala, J. Lee, J. C. Sadighian, E. Mosconi, R. Shivanna, E. Radicchi, M. Jeong, C. Yang, H. Choi, S. H. Park, M. H. Song, F. De Angelis, C. Y. Wong, R. H. Friend, B. R. Lee and H. J. Snaith, Ligand-engineered bandgap stability in mixed-halide perovskite LEDs, *Nature*, 2021, **591**(7848), 72–77.

27 G. B. Deacon and R. J. Phillips, Relationships between the carbon-oxygen stretching frequencies of carboxylato complexes and the type of carboxylate coordination, *Coord. Chem. Rev.*, 1980, **33**(3), 227–250.

28 X. Li, Y. Wu, S. Zhang, B. Cai, Y. Gu, J. Song and H. Zeng, $CsPbX_3$ quantum dots for lighting and displays: room-temperature synthesis, photoluminescence superiorities, underlying origins and white light-emitting diodes, *Adv. Funct. Mater.*, 2016, **26**(15), 2435–2445.

29 Y. Wu, C. Wei, X. Li, Y. Li, S. Qiu, W. Shen, B. Cai, Z. Sun, D. Yang, Z. Deng and H. Zeng, In situ passivation of $PbBr_6^{4-}$ octahedra toward blue luminescent $CsPbBr_3$ nanoplatelets with near 100% absolute quantum yield, *ACS Energy Lett.*, 2018, **3**(9), 2030–2037.

30 X. Wu, M. T. Trinh, D. Niesner, H. Zhu, Z. Norman, J. S. Owen, O. Yaffe, B. J. Kudisch and X. Y. Zhu, Trap states in lead iodide perovskites, *J. Am. Chem. Soc.*, 2015, **137**(5), 2089–2096.

31 A. Ito, K. Kamogawa, H. Sakai, K. Hamano, Y. Kondo, N. Yoshino and M. Abe, Micelle aggregating condition of fluorocarbon–hydrocarbon hybrid surfactants in aqueous solution, *Langmuir*, 1997, **13**(11), 2935–2942.

32 Y. Huang, Y. Feng, F. Li, F. Lin, Y. Wang, X. Chen and R. Xie, Sensing studies and applications based on metal halide perovskite materials: current advances and future perspectives, *Trends Anal. Chem.*, 2021, **134**, 116127.

33 S. Cinti, L. Fiore, R. Massoud, C. Cortese, D. Moscone, G. Palleschi and F. Arduini, Low-cost and reagent-free paper-based device to detect chloride ions in serum and sweat, *Talanta*, 2018, **179**, 186–192.

34 X. He, Y. Gu, B. Yu, Z. Liu, K. Zhu, N. Wu, X. Zhao, Y. Wei, J. Zhou and Y. Song, Multi-mode structural-color anti-counterfeiting labels based on physically unclonable amorphous photonic structures with convenient artificial intelligence authentication, *J. Mater. Chem. C*, 2019, **7**(45), 14069–14074.

35 M. Jin, L. Jiang, M. Lu and S. Bai, Monitoring chloride ion penetration in concrete structure based on the conductivity of graphene/cement composite, *Constr. Build. Mater.*, 2017, **136**, 394–404.

36 F. M. Li, Y. F. Feng, Y. P. Huang, Q. H. Yao, G. H. Huang, Y. M. Zhu and X. Chen, Colorimetric sensing of chloride in sweat based on fluorescence wavelength shift via halide exchange of $CsPbBr_3$ perovskite nanocrystals, *Microchim. Acta*, 2021, **188**, 2–8.

 This journal is © the Partner Organisations 2023